Functionally Electrospun PLA/Tubular Clay Nanocomposites for the Potential Application of Drug Delivery

Y. Dong
Department of Mechanical Engineering, Curtin University of Technology, Perth WA 6845, Australia
D. Chaudhary
Department of Chemical Engineering, Curtin University of Technology, Perth WA 6845, Australia
H. Haroosh
Department of Chemical Engineering, Curtin University of Technology, Perth WA 6845, Australia
V. Sharma
Department of Mechanical Engineering, Curtin University of Technology, Perth WA 6845, Australia
T. Bickford
Department of Mechanical Engineering, Curtin University of Technology, Perth WA 6845, Australia

Abstract

The electrospinning technique provides a simple but innovative approach to produce the non–woven fabrics consisting of fibrous structures on the order of usually 50–500 nanometres with quite large surface areas. Such electrospun nanofibres could be potentially used as multifunctional materials for a variety of applications including drug delivery, bio-scaffolding, industrial filtration, material reinforcements, military protection clothing, nanosensors and electronic devices. This paper introduces a novel material formulation method of poly (L-lactic acid) (PLA)/tubular clay nanocomposites via electrospinning to investigate the feasibility of tubular clay as the possible carrier for the drug delivery, due to its hollow structure. The important processing parameters such as solution concentration, weight fraction of tubular clays and feed rate of syringe pump were particularly investigated. Subsequently, the physical diameter of produced nanofibres, the dispersability of tubular clay and the thermal properties of related fabrics were then characterised by using the scanning electron microscopy (SEM), wide-angle X-ray diffraction (WAXD) and differential scanning calorimetry (DSC), respectively. A fundamental relationship to correlate the physical and thermal properties of

nanofibres with their structures was established in order to offer the better insight for the future application.

Introduction

Electrospinning of polymer solutions is a quite versatile process to fabricate ultrafine micro/nanofibrous structures in the form of non-woven fabrics. They could be potentially used in the effective drug delivery, tissue scaffolding, nanofiltration system, cosmetics and so on [1, 2]. When the solution jet is released, an electrostatic force due to the positive charge overcomes the surface tension to elongate the polymer droplets into charged polymer fibres which are further attracted to the earth ground collector. Generally a cone-like structure is generated at the tip of the capillary, widely known as a Taylor cone [3].

Base polymers such as polylactic acid (PLA), polycaprolactone (PCL), polyvinyl alcohol (PVA), polymethyl methacrylate (PMMA), etc have been widely used in electrospinning. Recent studies focus more on their counterpart composites like PVA/silica composites, PCL/metal composites, nylon 6/clay composites to benefit from their multifunctional properties, especially the reinforcement effect [1, 2]. Halloysite tubular clay ($Al_2Si_2O_5(OH)_4 \cdot nH_2O$) is one of unique inorganic fillers similar to kaolin, which shows a longitudinal hollow structure by rolling the layers of tetrahedral sheets of silica and octahedral sheets of alumina, and resemble carbon nantubes (CNTs) in geometry with relatively low cost [4, 5]. Extensive research work has been investigated in mechanical and microstructural properties [6-8], fracture behaviour [8], fire retardancy [9] and thermal properties [7, 10] of polymer/ tubular clay nanocomposites. However, the combined process of electrospinning tubular clay filled nanocomposites is still at the infant stage with very limited work [11], particularly targeting the drug delivery application.

This paper describes a preliminary study on the use of tubular clay as a potential carrier for drug delivery by understanding processing and material parameters, the analysis of microstructural and thermal properties of electrospun PLA/tubular clay nanocomposites. It is anticipated that it could eventually shed light on achieving the uniform nanofibrous structures as well as good clay dispersion.

Experimental work

Materials and fabrication process

Natureworks® PLA (Grade 3051D) pellets for injection moulding application were purchased from Jamplast Inc. (Ellisville, MO USA). The ultrafine premium

halloysite tubular clay particles were donated by Imerys Tableware Asia Limited, New Zealand. Dichloromethane (DCM) was employed to dissolve the PLA along with the additional solvent dimethyl formamide (DMF) to enhance the solution electric conductivity.

PLA pellets were mixed with DCM and DMF in a fixed ratio of 3:1 at room temperature by a bench top orbital shaking incubator for about 3 hrs in order to achieve the PLA solution concentrations of 8 and 12 wt%/v, respectively. As-received tubular clays were ultrasonicated for 20 min in DCM solvent which was subsequently evaporated by a hot plate magnetic mixer. Different clay contents ranging from 0.5, 1, 3 to 5 wt% were used in this study.

The electrospinning process was conducted by loading the prepared solution into a 10 ml plastic syringe with the luer lock tip to which a 21 gauge hypodermic metal needle was attached. A Fusion 100 syringe pump (Chemyx Inc. Stafford, TX USA) was operated to control the solution flow at constant feed rates of 1, 2 and 3 ml/hr. The positive electrode of a ES30P–5W high voltage power supply (Gamma High Voltage Research, Ormond Beach, FL USA) running at 25 kV was fixed with the needle via a crocodile clip; whereas a mesh collector covered by aluminium foil was connected to the earth ground point. The distance between the needle tip and the collector was kept at 14 cm. The entire setup was placed in a transparent acrylic housing case surrounded by a fume cupboard to remove the solvents during electrospinning.

Microstructural and thermal characterisation

To examine intercalation level of tubular clays, wide angle X-ray diffraction (WAXD) analysis was carried out via Bruker D8 ADVANCE diffractometer (Germany) at 40 kV and 40 mA with Cu-k_α X-ray beam (wave length $\lambda = 0.1541$ nm). Fabric samples were scanned at 2θ from 5 to 40° in a step size of 0.02°/s.

The surface morphology of electrospun fibre fabrics was examined by using a Philips XL30 field emission scanning electron microscope at an accelerating voltage of 5 kV. The fabric samples were sputter coated with platinum. The SEM micrographs were further evaluated using an imaging analysis tool, ImageJ, developed by National Institutes of Health (NIH), USA to determine the average diameters of electrospun fibres. Approximately 25 fibres per micrograph were chosen and various locations on each fibre were examined in case that the dimensional non-uniformity of fibres might arise.

Thermal properties of all electrospun fabrics were determined via differential scanning calorimetry (PerkinElmer DSC 6000, Waltham, Massachusetts USA) from 30 to 200°C at the heating/cooling rate of 10°C/min. The temperature of DSC samples was maintained at 200°C in an isothermal condition for 5 min to eliminate

any thermal history. The heating, cooling and reheating cycles were programmed, and the glass transition temperature (T_g), cold crystallisation temperature (T_{cc}), melting temperature (T_m) and heat of fusion (ΔH_m) were measured from the second heating cycle. The degree of crystallinity (X_c) was calculated from [12]

$$X_c(\%) = \frac{\Delta H_m}{\Delta H_m^0} \times \frac{100}{w} \quad (1)$$

Where $\Delta H_m{}^0$ is the heat of fusion for a 100% crystalline PLA material ($\Delta H_m{}^0$ =93 J/g [13]) and w is the weight fraction of PLA in the prepared fabric sample.

Results and discussion

XRD analysis

In order to examine the clay content effect, the XRD patterns of as–received tubular clays, electrospun PLA (12%/v) as well as corresponding PLA/clay nanocomposites at the feed rate of 2 ml/hr with various clay contents from 0.5, 1, 3 to 5 wt% are demonstrated in Fig. 1. For tubular clays alone, three characteristic XRD peaks were detected at 2θ =12.10, 19.96 and 24.88°, which are corresponding to the reflection planes of (001), (020), (110) and (002) with d-spacing values of 0.731, 0.445 and 0.358 nm, respectively. Due to the existence of first peak (d_{001}= 0.731 nm) and absence of 10A˚ peak (2θ =8.76°) for hydrated particles, this type of tubular clay is also referred to as (7A˚)–Halloysite with almost fully dehydrated formation [6, 8, 14].

At a given PLA solution concentration of 12%/v and relatively low clay contents of below 3 wt%, no apparent sharp peaks occur for PLA/clay nanocomposites with very similar XRD patterns to that of pure PLA. The only distinction could be made based on a non–shifted XRD peak taking place with relative low intensity at 0.5 wt% filled PLA/clay nanocomposites as compared to that of clay at the same 2θ =26.63°. This phenomenon might be attributed to either insufficient diffraction effect or a lack of the formation of well–ordered clay structures at such low clay contents. Quite differently, the first and second reflection (001) peaks of 5 wt% PLA/clay nanocomposites are both shifted to higher angles at 2θ =12.41 and 16.81° with the decreased d-spacing values of 0.713 and 0.527 nm, respectively, which might suggest the formation of clay collapsed structure (or "de–intercalation"). Furthermore, the intensity of their second reflection (001) peak has been greatly enhanced possibly resulting in well–ordered large clay agglomerates as well. Conversely, the reflection (020), (110) peaks of such nanocomposites are located at

lower angle of 2θ=19.20° corresponding to relatively large d-spacing value of 0.462 nm in comparison to 0.445 nm for tubular clay. This result reflects the presence of a limited intercalated structure in the clay dispersion. A totally different sign is revealed for the reflection (002) peak where its d–spacing value of nanocomposites is almost comparable to that of tubular clay signifying the non–intercalation effect due to the minimal peak shift.

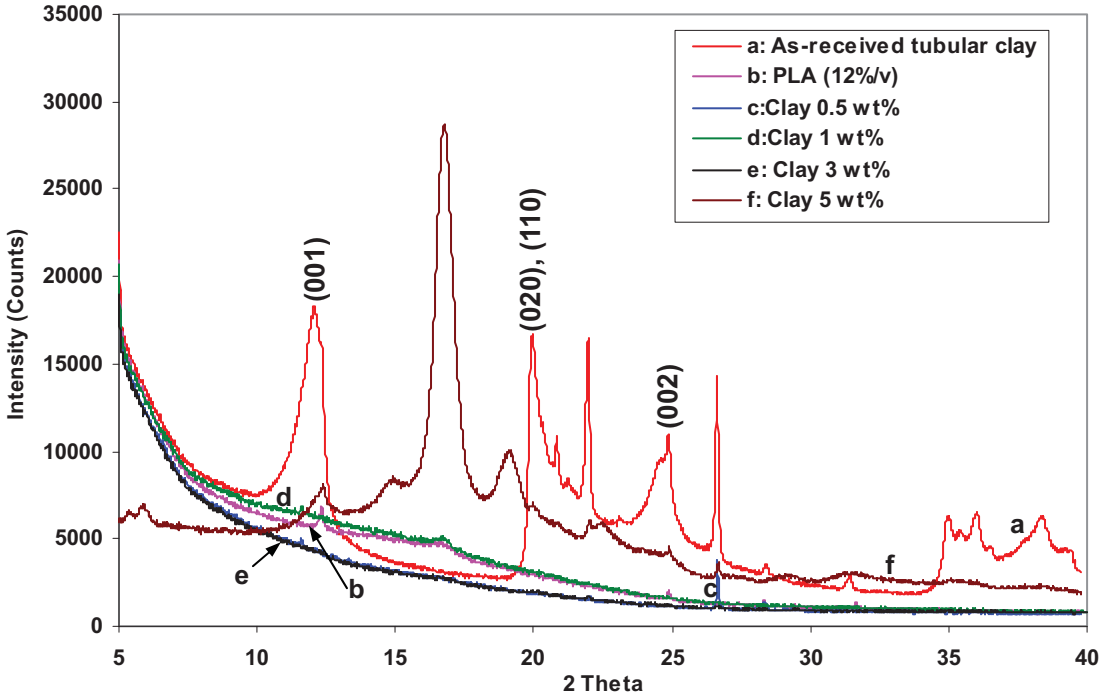

Fig. 1 XRD patterns of (a) as–received tubular clay, (b) electrospun PLA (12%/v) and corresponding electrospun PLA/clay nanocomposites at clay contents of (c) 0.5 wt%, (d) 1 wt%, (e) 3 wt% and (f) 5 wt%.

SEM characterisation

Fig. 2 demonstrates the different morphological structures of electrospun PLA/clay nanocomposites with the same material formulation used in aforementioned XRD analysis for the further investigation of clay content impact. At the additional clay contents of below 3 wt%, the majority of PLA/clay nanocomposites yield relatively small fibre diameter between 0.3 and 1μm, which could be attributed to both enhancements of electrical conductivity and viscosity of prepared solution due to the inclusion of tubular clay as proven elsewhere [15]. However, a certain degree of beads and agglomerates take place for nanocomposites containing 1 wt% clays. These noticeable defects are most likely due to the flow instability with the formation of droplet rather than fibrous structure [11]. On the other hand, the

significant fibre dimensional variation of electrospun nanocomposites has been clearly observed between 3 and 5 wt% clay inclusions. The fibre diameter of 3 wt% clay filled nanocomposites is ranging from 0.8 to 3 μm but the clay dispersion is still very uniform as opposed to 5 wt% nanocomposites; whereas large clay agglomerates and "slurry-like" unfavourable structure co-exist in the morphology of 5 wt% filled nanocomposites, along with non-woven entangled fibres with great diameter variations from 0.5 to 5 μm. Such visual clay aggregation here coincides with the finding of enhanced second reflection (001) peak intensity at the clay content of 5 wt%, Fig. 1. The "slurry-like" structure may be caused by excessive undispersed clay particles to prevent the solution jet from being elongated into fibrous formation.

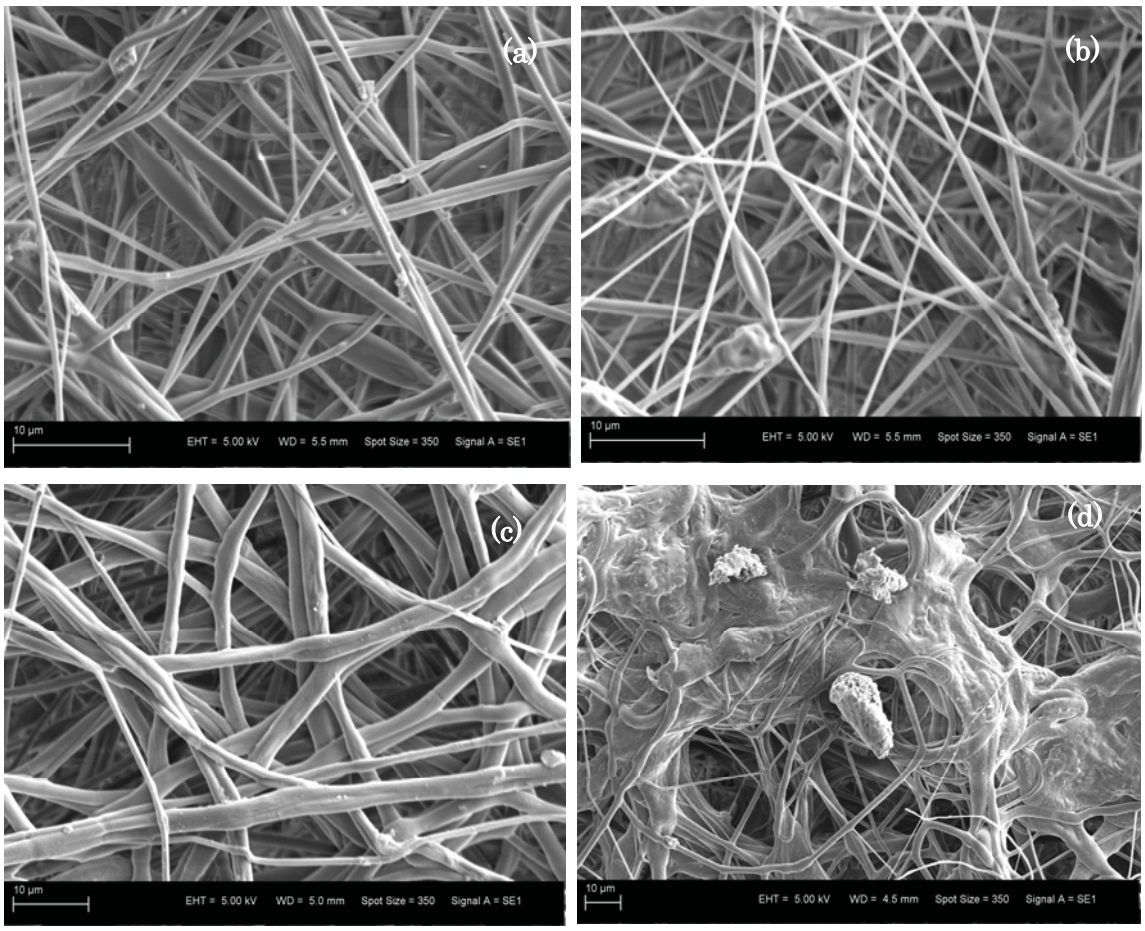

Fig. 2 SEM micrographs of PLA/tubular clay nanocomposites at varied clay contents (PLA: 12%/v and feed rate: 2 ml/hr): (a) 0.5 wt%, (b) 1 wt%, (c) 3 wt% and (d) 5 wt%.

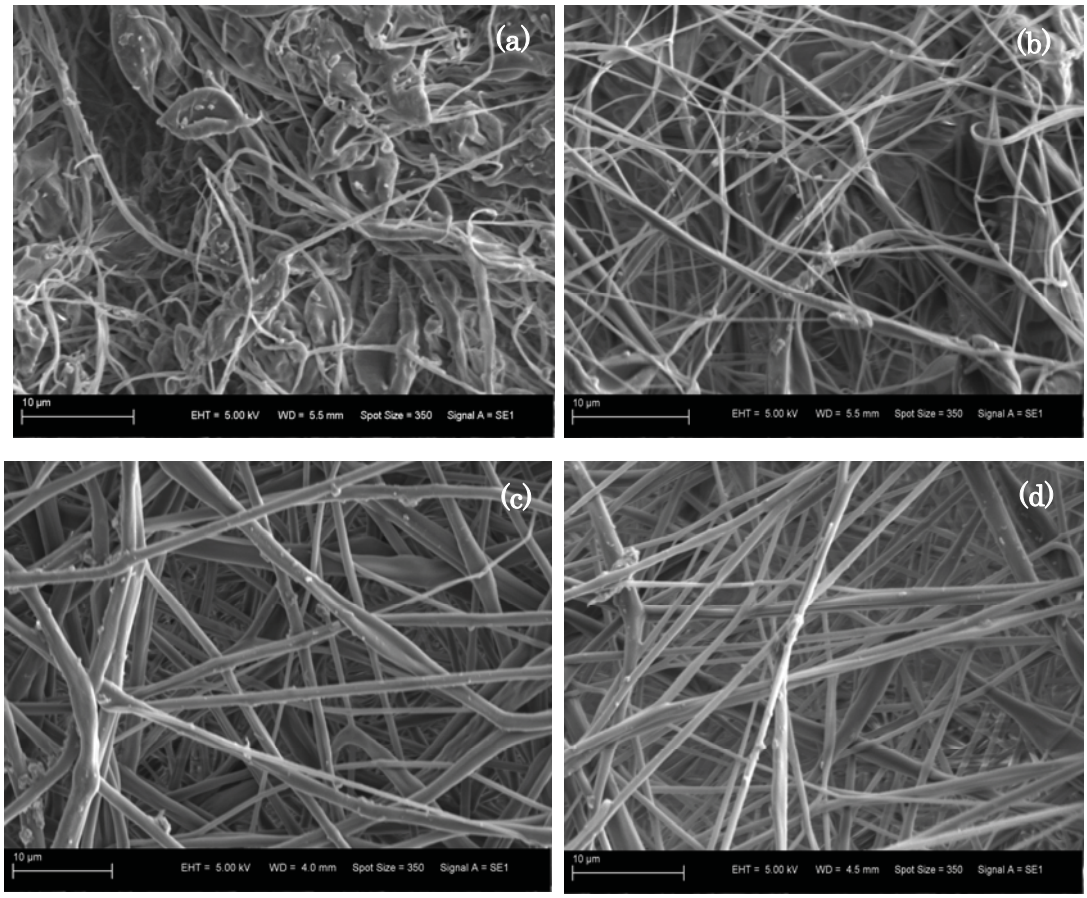

Fig. 3 SEM micrographs of 0.5% filled PLA/tubular clay nanocomposites at varied processing parameters: (a) PLA (8%/v) and feed rate of 1 ml/hr, (b) PLA (8%/v) and feed rate of 3 ml/hr,(c) PLA (12%/v) and feed rate of 1 ml/hr and (d) PLA (12%/v) and feed rate of 3 ml/hr.

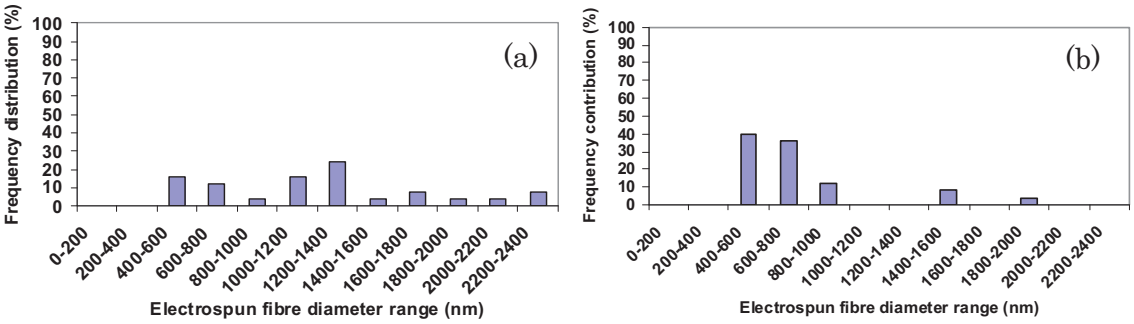

Fig. 4 Frequency distribution of electrospun 0.5 wt% filled PLA/clay nanocomposites (PLA: 12%/v) at varied feed rates: (a) 1 ml/hr and (b) 3 ml/hr.

Two major varied processing parameters were also studied in SEM analysis which comprise the solution concentrations of PLA (8%/v and 12%/v) and the feed rate (1, 2 and 3 ml/hr). A series of representative SEM micrographs were illustrated in Fig. 3 under various processing conditions for 0.5 wt% clay filled nanocomposites. The tubular clay particles in range of 200–800 nm for the lateral dimension were embedded into the electrospun fibres with good interfacial interactions and no clear de–bonding or pull-out of particles were found. However, some local clay agglomerates (less than 5 μm) are still visible as shown in Figs. 4 (b)–(d). At a given 8%/v for the PLA concentration, the bead formation was predominantly detected with the maximum lateral dimension of over 10 μm at the feed rate of 1 ml/hr. These large beads also concur with entangled fibrous structures down to the fibre diameter of less than 800 nm. More interestingly, the beads have greatly diminished despite relatively non–uniform fibrous structures at 3 ml/hr. When PLA concentration increases up to 12%/v, bead–free fibrous structures become quite manifested regardless of applied different feed rates, which might imply that the viscosity of polymer solution could have greater impact on the electrospun fibre quality as opposed to the feed rate. Taking that fact into consideration, Fig. 4 plots frequency distribution curves of average fibre diameter in nanocomposites only containing PLA solution concentration of 12%/v at feed rates of 1 and 3 ml/hr. To quantify the number of nanofibres with average fibre diameter below 1 μm, it occurs more frequently (shown in Figs. 4 (b)) in PLA/clay nanocomposites at feed rate of 3 ml/hr for which the frequency contribution of 88% have been achieved. In particular, more uniform nanofibres in range of 400 to 600 nm and 600 to 800 nm are prevalently detected at 3 ml/hr with the frequency contribution of 76%. On the contrary, electrospun PLA/clay nanocomposites at 1 ml/hr produced much lower number of nanofibres (Frequency contribution of 32 %), Figs. 4(a). A most widespread dimensional variation from 400 nm to 2.4 μm was found instead. It is implied that quite a low feed rate might potentially impede the flow stability of solution due to the existence of tubular clays and optimal feed rate of 3 ml/hr seems to be more feasible in such electrospinning processes.

DSC measurement

All DSC characteristic parameters of electrospun PLA (12%/v) and PLA/ clay nanocomposites at the clay contents from 0.5 to 5 wt% are summarised in Table 1. Similar glass transition temperatures were found for all DSC samples of PLA /clay nanocomposites regardless of the clay content, which are also comparable to that of PLA (T_g = 59.28°C). Cold crystallisation temperatures decrease remarkably to 114-117°C at the low clay contents (0.5 to 3 wt%) when compared with T_{cc} of PLA at 123.80°C. This behaviour can be explained by the effective nucleating agent role of

well dispersed clays as depicted in Figs. 2(a) and (c), thus having the strong interaction with the PLA matrix to enhance its nucleation level and crystal growth rate [16-18]. PLA molecules with a small amount of well dispersed additional clays are believed to facilitate the crystallisation process occurring at lower temperatures, resulting in the subsequent decrease of T_{cc}. Interesting to see, T_{cc} of such nanocomposites has drastically changed at the clay content of 5 wt% and even becomes slightly higher than that of PLA. The relatively high clay content might lead to constraints and partial immobilisation of a large number of PLA molecular chains by attaching to more individual clay particles [18]. The large clay agglomerates found in Fig. 2(d) as physical hindrance would also be detrimental to the PLA crystallisation process due to the non-homogeneous dispersion. The great improvements of degree of crystallinity (X_c) in 0.5–3 wt% filled PLA/clay nanocomposites were shown with nearly five fold values relative to 8.5% for PLA alone. These results agree quite well with those corresponding cold crystallisation temperatures, further proving the positive nucleation effect from tubular clays at low content levels. When the clay content increases up to 5 wt%, the degree of crystallinity (X_c =2.8%) is abruptly lowered. The melting temperatures (T_m) follow quite similar tendencies to the degree of crystallinity, being much higher for 0.5-3 wt% clay inclusions but remaining comparable to PLA at 5 wt%. This finding might shed light on the potential use of tubular clays to improve the thermal stability and inflammability level of PLA significantly as evidenced elsewhere [19,20].

Table 1 DSC characteristic parameters for PLA and PLA/clay nanocomposites

DSC samples	Clay content (wt %)	T_g (°C)	T_{cc} (°C)	T_m (°C)	ΔH_m (J/g)	X_c (%)
PLA (12%/v)	0	59.28	123.80	153.77	7.91	8.5
PLA (12%/v)/ clay (0.5 wt%)	0.5	60.20	114.49	169.38	35.18	38.0
PLA (12%/v)/ clay (1 wt%)	1	59.35	116.80	169.54	38.28	41.6
PLA (12%/v)/ clay (3 wt%)	3	60.10	115.79	170.98	38.72	42.9
PLA (12%/v)/ clay (5 wt%)	5	59.54	127.28	154.11	2.46	2.8

Conclusions

A novel material formulation in electrospinning process was developed by incorporating tubular clays at low content levels from 0.5 to 5 wt% with PLA. Such PLA/tubular clay nanocomposites show good clay dispersion for 0.5 to 3 wt% clay

inclusions as evidenced by weak XRD peaks and SEM morphological structures. At the clay content of 5 wt%, a complex dispersion status is yielded with de-intercalated, limited intercalated and non–intercalated effects taking place at reflection (001), (020), (110) and (002) peaks, respectively. In addition, large clay agglomerates and "slurry-like" unfavourable structure are confirmed in SEM analysis for 5 wt% filled nanocomposites as well. The study of varied processing parameters suggests that higher solution concentration of PLA (12%/v) and fast feed rate (3 ml/hr) contribute greatly to the dimensional uniformity and bead-free formation of fibrous structures. The enhancement of thermal properties such as melting temperature (T_m) and degree of crystallinity (X_c) is quite attractive for 0.5-3 wt% filled nanocomposites. The lower cold crystallization temperature (T_{cc}) at similar clay content levels is ascribed to the effective nucleating agent role of tubular clays. However, for nanocomposites containing 5 wt% clays, X_c and T_{cc} are drastically altered to reach a similar level to those for electrospun PLA, possibly arising from the non-uniform clay dispersion with relatively high clay content and large agglomerates. This work will offer a clear insight to shift the real applications of tubular clays from conventional reinforcements to drug delivery when both their hollow structure as potential carrier and electrospinning nanofibre technique are considered.

Acknowledgements

The authors would like to thank the financial supports from both Curtin Internal Research Grants (IRG) 2010 (Project No.: 47604) and New Staff Academic Development Fund from Curtin Engineering Faculty to Dr. Y. Dong. The technical assistance of XRD analysis from Prof. De Yu Li, Centre for Materials Research (CMR), Curtin University of Technology is also acknowledged.

References

1. Z.M. Huang, Y. Z. Zhang, M. Kotaki, S. Ramakrishna, Compos. Sci. Technol., 63, 2223-53 (2003).
2. S. Agarwal, J.H. Wendorff, A. Greiner, Polymer, 49, 5603-21 (2008).
3. R. Inai, M. Kotaki, S. Ramakrishna, Nanotechnology, 16, 208-13 (2005).
4. E. Joussein, S. Petit, J. Churchman, B. Theng, D. Righi, B. Delvaux, Clay Miner., 40, 383-426 (2005).
5. C.C. Harvey, H.H. Murray, Clay Miner. Soc. Spec. Pub., 1, 233-48 (1990).
6. H. Ismail, P. Pasbakhsh, M. N. Ahmad Fauzi, A. Abu Bakar, Polym.-Plast.

Technol. Eng., 48, 313-23 (2009).
7. H. Ismail, P. Pasbakhsh, M.N. Ahmad Fauzi, A. Abu Bakar, Polym. Test, 27, 841-50 (2008).
8. S. Deng, J. Zhang, L. Ye, Compos. Sci. Technol., 69, 2497–505 (2009).
9. D.C.O. Marney, L.J. Russell, D.Y. Wu, T. Nguyen, D. Crammb, N. Rigopoulos, N. Wright, M. Greaves, Polym. Degrad. Stabil., 93, 1971-8 (2008).
10. M. Liu, B. Guo, Q. Zou, M. Du, D. Jia, Nanotechnology, 19**,** 205709 (2008).
11. A. H. Touny, J.G. Lawrence, A.D. Jones, S.B. Bhaduri, J. Mater. Res., 25, 857-65 (2010).
12. A. P. Matthew, K. Oksman, M. Sain, J. Appl. Polym. Sci., 101, 300-10 (2006).
13. E. W. Fischer, H. J. Sterzel, G. Wegner, Z. Z. Kolloid, Polymer, 251, 980-90 (1973).
14. S.R. Levis, P.B. Deasy, Int. J. Pharm., 243, 125-34 (2002).
15. S.I. Marras, K.P. Kladi, I. Tsivintzelis, I. Zuburtikudis, and C. Panayiotou, Acta Biomater., 4, 756-65 (2008).
16. J. H. Lee, T. G. Park, S. H. Park, D. S. Lee, Y. K. Lee, S. C. Yoon, J. D. Nam, Biomaterial, 24, 2773-8 (2003).
17. W. S. Chow, S. K. Lok, J. Therm. Anal. Calorim., 95, 627-32 (2009).
18. Y. Di, S. Iannace, E. D. Maio, L. Nicolais, J. Polym. Sci. Pt. B-Polym. Phys., 43, 689-98 (2005).
19. N. Ning, Q. Yin, F. Luo, Q Zhang, R. Du, Q. Fu, Polymer, 48, 7374-84 (2007).
20. M. Du, B. Guo, D. Jia, Eur. Polym. J. 42, 1362-9 (2006).